Received 24 February 2023; revised 26 April 2023; accepted 3 May 2023. Date of publication 10 May 2023; date of current version 23 May 2023.

Digital Object Identifier 10.1109/OJAP.2023.3274782

3-D Printable Synthetic Metasurface to Realize 2-D Beam-Steering Antenna

FOEZ AHMED [1] (Member, IEEE), TOUSEEF HAYAT [2] (Graduate Student Member, IEEE), MUHAMMAD U. AFZAL [1] (Senior Member, IEEE), SHIYU ZHANG [3], KARU P. ESSELLE [1] (Fellow, IEEE), AND WILLIAM G. WHITTOW [3] (Senior Member, IEEE)

[1]School of Electrical and Data Engineering, University of Technology Sydney, Sydney, NSW 2007, Australia

[2]School of Engineering, Macquarie University, Sydney, NSW 2113, Australia

[3]Wolfson School of Mechanical, Electrical and Manufacturing Engineering, Loughborough University, LE11 3TU Loughborough, U.K.

CORRESPONDING AUTHOR: F. AHMED (e-mail: foez.ahmed@student.uts.edu.au)

This work was supported in part by The Post Thesis Scholarship, University of Technology Sydney; in part by the Australian Research Council Discovery Grant; and in part by EPSRC under Grant "SYMETA" EP/N010493/1 and Grant "ANISAT" EP/S030301/1.

ABSTRACT This article presents highly radio-frequency (RF) transparent phase gradient synthetic metasurfaces made of sub-wavelength-sized 3D printable meta-atoms with tailored permittivity that cannot be achieved with off-the-shelf, commercially available materials. The synthesized meta-atoms design uses one dielectric block of PREPERM®ABS 1000 material with air and metallic inclusions to make low- and high-permittivity materials. The inclusions' size and height are varied to achieve a complete phase range from 0 to 360°, while maintaining transmission magnitudes greater than −3.0 dB. A two-dimensional array of meta-atoms forms a metasurface, which can be used for phase-shifting structures. Such metasurfaces can manipulate RF waves by introducing progressive phase delay into array elements. The proposed meta-atoms are employed to create highly RF transparent phase-gradient metal-dielectric composite metasurfaces (MDCMs) operating at 11 GHz. These MDCMs can be implemented through 3D printed technology using low-cost thermoplastics or polymers with composite filaments and minimal human intervention. A pair of MDCMs are combined with an array of microstrip patches to demonstrate 2D beam steering functionality numerically. The antenna system provides a peak directivity of 19.9 dBi with a maximum conical scanning angle of 114° and a directivity variation of less than 3 dB.

INDEX TERMS 3D printed, acrylonitrile butadiene styrene, additive manufacturing, beam steering, near-field meta-steering, non-homogenous, phase-shifting surface, phased arrays, rapid prototyping, synthetic metasurface.

I. INTRODUCTION

CUSTOMIZED electromagnetic (EM) response with two-dimensional (2D) metasurfaces has been a topic of considerable interest among the research community. Their ability to modify the phase of the propagating EM fields makes them suitable for beam-steering antennas desired for the next generation of wireless standards [1], [2], [3], [4]. However, the capability of the metasurfaces cannot be fully utilized in physical prototypes with commercial off-the-shelf (COTS) materials that come with preset effective permittivity and permeability [5], [6]. Subsequently, the recent development on metasurfaces has seen an alternative approach to artificially achieving the equivalent characteristics through the inclusion of impurities in host materials that offer greater flexibility to incorporate metasurfaces in practical systems [7], [8].

The widely adopted strategy to realize metasurfaces is to first design their fundamental repeating blocks, referred to as "meta-atoms". A few challenges are evident in the fabrication of meta-atoms and, subsequently, metasurfaces, principally the difficulty in fabricating micro- and nano-three-dimensional structures with unrealistic overhangs using

traditional machining techniques like lithography and nano-printing that involve tedious machining and bonding steps, which in turn escalate the component cost [9], [10], [11]. Moreover, because of strong dispersion and high losses, traditional materials are inadequate to design beam-steering metasurfaces with high transmission magnitude [9], [12].

Additive manufacturing (AM), also known as 3D printing technology, is rapidly taking the place of traditional manufacturing because of its many advantages, including low cost, rapid prototyping, automated manufacturing, and repeatability [10], [13], [14], [15]. It can produce extremely customized metasurfaces for state-of-the-art applications that can meet the stringent benchmarks of modern communication systems. Heterogeneous metamaterials that are otherwise difficult to fabricate using traditional micro-machining with modified geometries can be efficiently manufactured by the AM technique. Moreover, because bonding and machining are not involved, the AM techniques make design inherently robust for even complex environments [16].

In this article, we investigate and present highly transparent, low-cost 3D printable meta-atoms to create metasurfaces that can achieve continuous permittivity within a fixed permittivity range. Two separate techniques are presented to achieve low- and high-permittivity meta-atoms by embedding air and metal inclusions in a single dielectric. The effective parameters (permittivity and permeability) of the proposed meta-atoms are calculated using the S-parameter retrieval method. These meta-atoms can be synthesized for any permittivity value between 2.6 and 21.4 using PREPERM®ABS 1000 filament as a base material, which has a base permittivity of 10 [17]. It is to be noted here that for phase-transforming metasurfaces, the meta-atoms must be able to achieve complete 2π phase shifts, which are achieved here by varying the heights of the two meta-atoms.

The meta-atoms are arranged with gradient phase delay to form a 3D printable metal-dielectric composite metasurface (MDCM) for steering the beam of a patch array antenna. With a pair of MDCMs, the broadside beam of a patch array is steered in a conical region having an apex angle of 114° by the mutual physical rotation of two metasurfaces following the concept of Risley prism [18], [19]. The proposed MDCMs are superior in characteristics compared to previously reported all-dielectric and all-metal near-field phase transforming structures [20], [21], [22], [23], [24], which have their respective limitations pertaining to excessive height, ohmic losses, and fabrication complexity. The maximum height of MDCM is 9.8 mm ($\approx 0.36\lambda_0$, where λ_0 is the wavelength at the operating frequency of 11 GHz), which is 88.7% shorter than the all-dielectric structure reported in [20], which would have a maximum height of 31.9 mm ($3.19\lambda_0$). The maximum lateral dimension of metal inclusion in each periodic meta-atom is limited to 3.4 mm, which is 43% of the meta-atom's total area, to keep the ohmic losses less than −3.0 dB. The phase-transforming structure reported in [21] needs to be constructed using at least four separate 3D filaments and very accurate micro-milling techniques. Moreover, our proposed MDCM is thinner, polarization-insensitive, and has a broader range of permittivity values as opposed to the $2.4\lambda_c$ thick and polarization-dependent gradient index lens with limited permittivity values demonstrated in [25] for beam-steering application. In contrast, conventional thin-printed metasurfaces need more than one metal layer (at least three) to achieve a similar level of performance in terms of transmission magnitude, and phase range [3]. The proposed 3D-printed design approach is free from that and also evades multi-layer air-metal structures [22], [23], [24], [26] to attain a higher transmission magnitude.

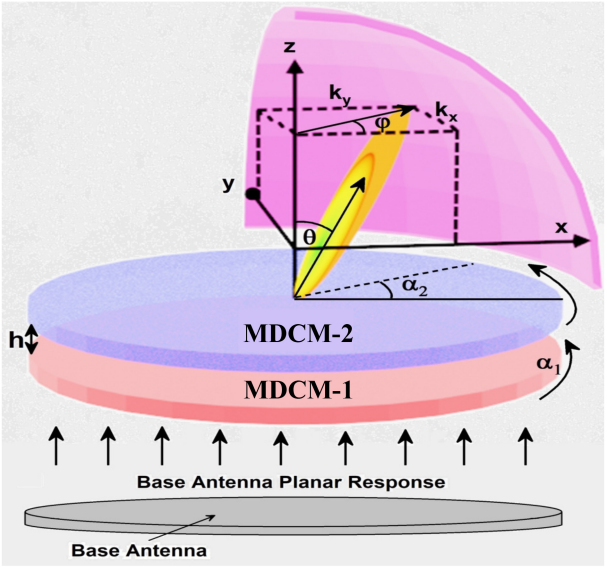

FIGURE 1. Configuration of a beam-steering antenna system comprising a pair of MDCMs placed above the feed antenna.

The rest of the paper is organized as follows. Section II describes the mechanism that is employed to steer the beam in both azimuth and elevation using a pair of MDCMs. The S-parameter retrieval method and design of low- and high-permittivity materials that form the basis of MDCM are explained in Section III. The design of MDCM is explained in Section IV. Results are discussed in Section V, and a conclusion is given in Section VI.

II. BEAM-STEERING MECHANISM

The configuration of the beam-steering antenna system is shown in Fig. 1. It has a fixed-beam static base antenna at the bottom with a large radiating aperture and a pair of independently rotatable MDCMs atop; each MDCM is separated by a fraction of the free-space wavelength (4 mm or $0.15\lambda_0$). The closely packed array of patches radiates electric fields with uniform phase distribution in the near-field region, while the MDCMs, which fully cover the antenna aperture, transform the phase of the propagating electric fields. In the classical configuration, MDCMs are designed such that they change the direction of radiated field propagation from broadside to an offset angle δ by introducing a gradient in the phase of

the electric fields. Thus, when used separately with the base antenna, each MDCM tilts the antenna beam by an angle of δ. If a single MDCM is placed above the base antenna and rotated, its tilted beam with a fixed elevation angle can be moved to any azimuth angle between 0° and 360°. The combination of two MDCMs gives freedom to steer the beam in both elevation and azimuth planes in a conical region having an apex angle of at least 2δ. Such beam-steering mechanisms also known as meta-steering antenna systems, are described in detail in [3], [21], [23], [27], [28]. The steering aspects are, however, briefly explained below with analytical and numerical examples to assist in better understanding.

The beam direction for any rotational combination of MDCMs can be predicted with an analytical method using the design parameters of the MDCMs and antenna system. The beam tilt angles of the MDCM-1 and MDCM-2 are represented by δ_1 and δ_2, while their respective rotation angles measured in an anticlockwise direction from the x-axis are represented by α_1 and α_2 [27]. The tilt angle of the MDCM is related to the phase delay gradient (p_i) introduced in the phase of the electric field while propagating through the metasurface as follows:

$$p_i = sin\delta_i \times k_0 \tag{1}$$

where δ_i is the tilt angle of the surface and $k_0 = 2\pi/\lambda_0$ is the wavenumber in free space, and λ_0 is free space-wavelength at the operating frequency.

The wave propagating in the direction of the antenna beam has two projected wavenumbers: k_x and k_y in the direction of unit vectors $\hat{\boldsymbol{x}}$ and $\hat{\boldsymbol{y}}$, respectively. The wavenumbers are related to phase-delay gradients, and physical rotation angles of the MDCMs as follows [27].

$$k_x = p_1 cos\alpha_1 + p_2 cos\alpha_2 \tag{2a}$$
$$k_y = p_1 sin\alpha_1 + p_2 sin\alpha_2 \tag{2b}$$

The resultant azimuth (ϕ) and elevation angles (θ) can be calculated using the wavenumbers, given by

$$\theta = sin^{-1}\left(\frac{\sqrt{k_x^2 + k_y^2}}{k_0}\right) \tag{3a}$$
$$\phi = tan^{-1}\frac{k_y}{k_x} \tag{3b}$$

The equations can be further simplified by substituting (2a) and (2b) in (3a) and (3b).

$$\theta = sin^{-1}\left[\frac{1}{k}\left[p_1^2 + p_2^2 + 2p_1p_2\cos(\alpha_1 - \alpha_2)\right]^{1/2}\right] \tag{4}$$
$$\phi = tan^{-1}\left(\frac{p_1 sin\alpha_1 + p_2 sin\alpha_2}{p_1 cos\alpha_1 + p_2 cos\alpha_2}\right) \tag{5}$$

Using (4) and (5), the elevation and azimuth angles of the output beam can be analytically estimated by appropriately choosing the rotation angles of the two MDCMs while the base antenna is absolutely fixed.

TABLE 1. The estimated beam positions in azimuth and elevation planes. MDCM-1 is stationary at $\alpha_1 = 0°$ and MDCM-2 is rotated from $\alpha_2 = 30°$ to 180° in steps of 30°.

$\alpha_1(°)$	$\alpha_2(°)$	$\theta(°)$	$\phi(°)$
0	30	58	15
0	60	49	30
0	90	38	45
0	120	26	60
0	150	13	75
0	180	0	90

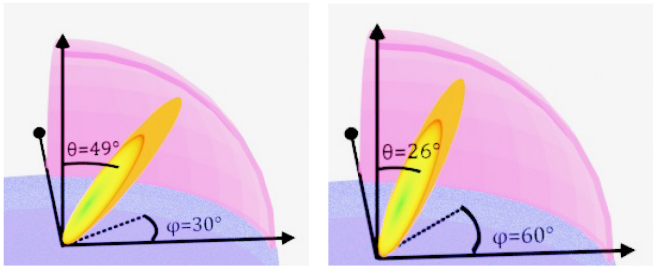

(a) (b)

FIGURE 2. Depiction of antenna beam direction in elevation (θ) and azimuth (ϕ) planes when MDCM-1 is fixed and MDCM-2 is rotated in counter-clockwise directions at (a) $\alpha_2 = 60°$ and (b) $\alpha_2 = 120°$.

Consider a numerical example, where MDCMs have the same tilt angles of $\delta_1 = \delta_2 = 26°$ and the antenna operates at the frequency of 11 GHz. The phase-delay gradients p_1 and p_2 of the two MDCMs, calculated using (1), are 5.77 deg/m. The MDCM-1 is fixed along the x-axis (i.e., $\alpha_1 = 0°$) and the MDCM-2 is rotated between 30° and 180° in a counter-clockwise direction in steps of 30°. The resultant beam positions for all seven orientations of the MDCMs calculated using (4) and (5) are given in Table 1.

In a special case, when $\alpha_1 = \alpha_2 = 0°$ and $k_y = 0$, the resultant beam is scanned to the farthest elevation angle, i.e., $\theta = \theta_{max} = 61.16°$ and at the azimuth angle of $\phi = 0°$. With the counter-clockwise rotation of MDCM-2, both projection components change the beam location, and the azimuth angle follows a sinusoidal path. When $\alpha_1 = 0°$ and $\alpha_2 = 180°$, both projection components are nullified, and the beam points in the broadside direction. As a demonstration, beam positions for two different cases where $\alpha_2 = 60°$ and $\alpha_2 = 120°$ are shown in Fig. 2. The following section explains the design details of meta-atoms with air, dielectric, and metal composites, which can be arranged with gradient phase delay to develop MDCMs for beam-steering applications.

III. META-ATOM DESIGN AND CHARACTERIZATION

Meta-atoms are the basic building blocks of MDCMs, and they must have a continuous permittivity between 1 and $\epsilon_r(max)$. This is accomplished through the use of two distinct meta-atoms made of dielectric material with an intermediate base permittivity, ϵ_b. The first meta-atom, referred to as

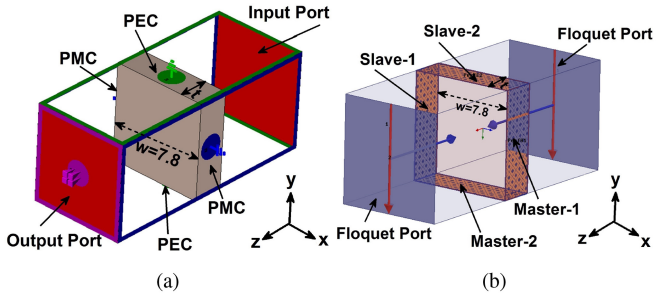

FIGURE 3. Perspective view of dielectric blocks modeled in (a) CST and (b) HFSS solvers for S-parameter extraction.

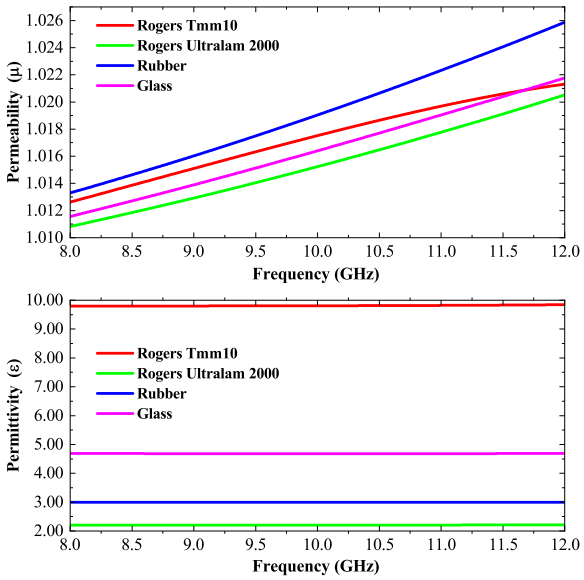

FIGURE 4. The estimated relative permittivity and permeability obtained from full-wave meta-atom simulations.

M1 hereafter, covers the lower permittivity range from 1 to ϵ_b, while M2, the second meta-atom, covers the permittivity range from ϵ_b to $\epsilon_{r(max)}$.

The effective permittivity of meta-atoms, particularly at higher frequencies, can be derived either by the analytical Drude-Lorentz model [29] or by the scattering parameter (S-parameter) retrieval method [30], [31], [32]. For complex, inhomogeneous meta-atoms with multiple material composites, the former is less accurate and unreliable. Contrary to this, the S-parameter retrieval method is more accurate, as it extracts reflections and transmissions through full-wave simulations of actual meta-atoms. This method is used here, where the S-parameters of the meta-atoms are retrieved with two independent commercial EM simulators: the finite integration technique (FIT)-based CST Microwave Studio and the finite element method (FEM)-based high-frequency structure simulator (HFSS).

The meta-atoms are simulated with meta-atom boundary conditions to extract the S-parameter. The meta-atom conditions are realized using periodic boundaries and master-slave boundaries in two lateral directions in CST and HFSS, respectively [33]. They are excited by the plane wave propagating in the longitudinal direction along the $+z$-axis. The pictorial representation of two meta-atom models is shown in Fig. 3 (a) and (b), respectively. The extracted S-parameters are then used to estimate the effective permittivity and permeability of the meta-atoms over a wider frequency band via numerical methods [33]. First, the effective refractive index (n) and intrinsic impedance (z) are calculated from retrieved S-parameters using (6) and (7).

$$z = \pm\sqrt{\frac{(1+S_{11})^2 - S_{21}^2}{(1-S_{11})^2 - S_{21}^2}} \tag{6}$$

$$e^{ink_0d} = X \pm i\sqrt{1-X^2} \tag{7}$$

where, $X = 1/2S_{21}(1 - S_{11}^2 + S_{21}^2)$. Since the metamaterial under consideration is a passive medium, the signs in (6) and (7) are determined based on the following conditions [31]:

$$z' \geq 0 \tag{8a}$$

$$n'' \geq 0 \tag{8b}$$

where (.)′ and (.)″ denote the real part and imaginary part of operators, respectively. The value of refractive index n can be determined from (7) as follows:

$$n = \frac{1}{k_0 d}\left[\left[\left[\ln\left(e^{\imath nk_0 d}\right)\right]'' + 2m\Pi\right] - \imath\left[ln\left(e^{\imath nk_0 d}\right)\right]'\right] \tag{9}$$

Since we have considered the case of a homogeneous slab for which the boundaries of the slab are well defined along the direction of propagation of a plane wave, the S-parameters are accurately known. So, effective parameters of the slab can be calculated directly from n and z using (10) and (11) [31].

$$\varepsilon = \frac{n}{z} \tag{10}$$

$$\mu = n \times z \tag{11}$$

The method is verified with a meta-atom made out of four different dielectrics with known permittivities: Rogers TMM10, Rogers RT5880, rubber, and glass. The permittivity values for four cases are estimated through the S-parameter retrieval method and compared with actual values. The meta-atom used for analysis in both simulation environments is a square block with length $w = 7.8$ mm ($\lambda_0/3.5$) and thickness (t) of 2.5 mm. The estimated effective permittivity and permeability of meta-atoms in the frequency range from 8 to 12 GHz are plotted in Fig. 4. The method is extended to estimate the effective characteristics of M1 and M2, which are explained in the following two subsections.

A. META-ATOM I (M1) WITH AIR INCLUSIONS

The meta-atom, M1 is designed to attain permittivity values between 1 and ϵ_b. This is achieved using a dielectric material with an air inclusion, as shown in Fig. 5 (a). The width of the

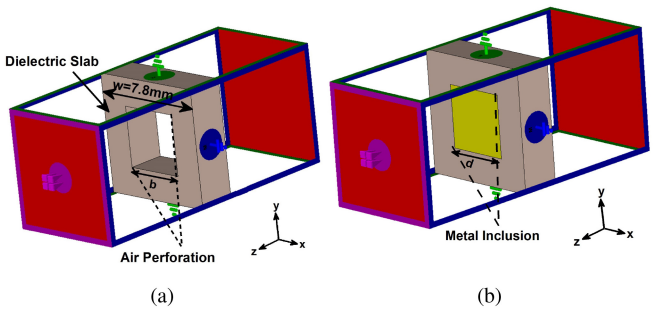

FIGURE 5. Meta-atom models in full-wave simulations (a) M1: low-permittivity materials by introducing air perforation, and (b) M2: high-permittivity materials by introducing metal inclusion in the host dielectric.

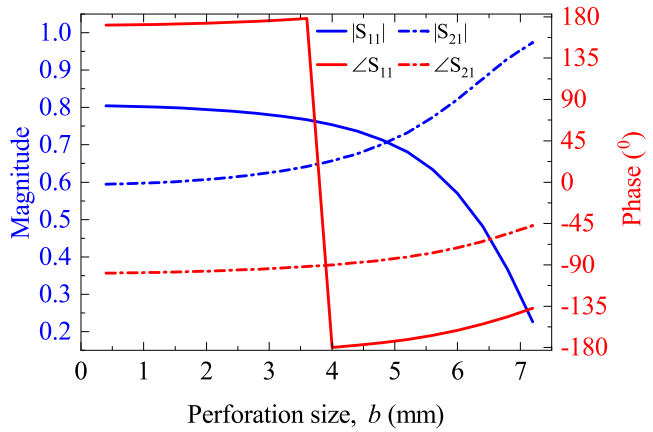

FIGURE 6. Predicted S-parameters by changing the perforation size in 7.8 mm cell made of PREPERM®ABS 1000.

dielectric is w, and that of air inclusion is b. The 3D printable dielectric material used with M1 is PREPERM®ABS 1000, which has a base permittivity (ϵ_b) of 10. The effective permittivity of the meta-atom is reduced below 10 by increasing the size of the air inclusion [34]. It is noted that if traditional machining methods are used to introduce air inclusions, the drill bits available are of discrete sizes, and hence discrete effective permittivity values can only be achieved. To achieve continuous effective permittivity between 2.6 and 10, additive manufacturing can be used instead, which can provide accuracy at the sub-millimeter level to realize M1 with desired permittivity values [8].

Contemporary 3D printing tools equip nozzles with diameters of as little as 0.3 – 0.4 mm and printers that can print the layer height of as thin as 0.1 mm. So they offer huge customization capabilities for the design of non-homogeneous materials. Furthermore, square perforations instead of conventional cylindrical perforations are easy to realize using 3D printing [34], as square drill bits are nonexistent. Given the most common printing nozzle size of 0.4 mm, the perforation size in M1 can be adjusted in steps of 0.4 mm between 0 mm and 7.2 mm. S-parameters were computed for each perforation size with full-wave simulations, which are plotted in Fig. 6. As the perforation's size increases, the dielectric volume decreases, resulting in less dielectric

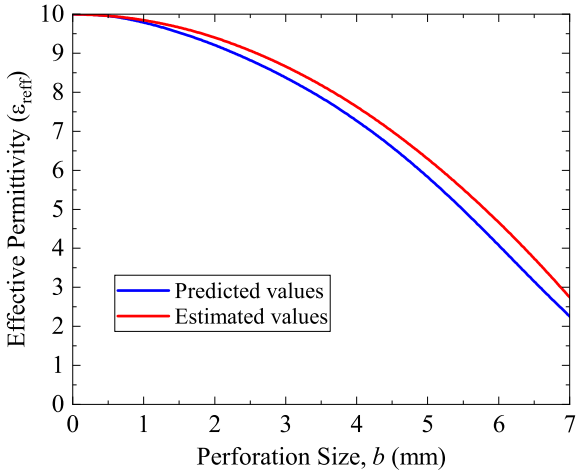

FIGURE 7. Comparison of effective permittivity obtained through full-wave simulations and estimated using (10) with various perforation sizes in 7.8 mm meta-atoms.

losses. Thus, the insertion loss is minimal, which significantly enhances the transmission. The effective permittivity was calculated using (10) and is plotted in Fig. 7. The calculated permittivity values for M1 are compared with the theoretically expected values estimated by the volumetric average of the dielectric and air in the meta-atom structure [34]. The two curves tracked each other closely, and the M1 was able to achieve continuous permittivity values from 2.6 to 10.

B. META-ATOM II (M2) WITH METAL INCLUSIONS

The configuration of M2 is shown in Fig. 5 (b), where a metal block of size d is printed into the host dielectric. The thickness (or height) of the metal block is chosen to be the same as that of the dielectric. The M2 has a continuous effective permittivity between ϵ_b and $\epsilon_r(max)$. Traditionally, high permittivity artificial materials are engineered by mounting multiple metal and dielectric layers, which are unrealistic to realize using 3D printing as no class of printers can handle both metals and dielectrics simultaneously [8]. The rationale for using a solid metal block in M2 instead of the metal and dielectric layers conventionally used is that such an arrangement can be realized at a low cost with additive manufacturing.

The boundaries of the proposed meta-atom are well defined in the direction of wave propagation (z-axis), so (10) and (11) can be applied directly without sign ambiguities to calculate the effective parameters. This contrasts with the split ring resonator (SRR) meta-atom, which has multiple metal and dielectric layers in the direction of incident wave propagation, resulting in sign ambiguity during the calculation of its effective parameters [31].

In M2, the size of the metal inclusion controls effective permittivity and insertion loss. If the size of the metal inclusion is comparable to the local periodicity of the meta-atom, the reflections are too high to be useful for transmitting

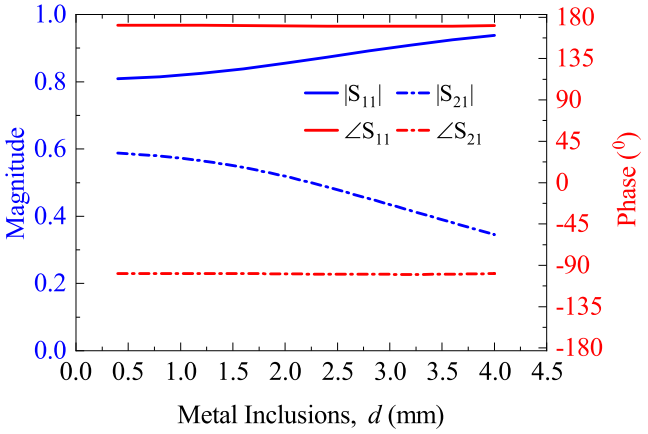

FIGURE 8. Predicted S-parameters by varying the size of metal inclusions in PREPERM®ABS 1000.

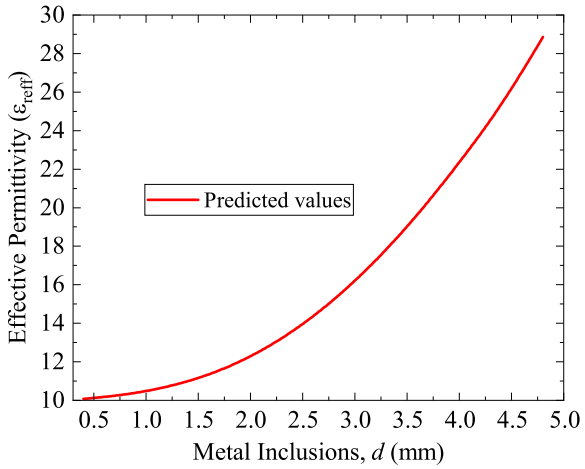

FIGURE 9. Effective permittivity value by varying the size of metal inclusion in PREPERM®ABS 1000.

metasurfaces. The M2 was simulated using periodic boundary conditions similar to the M1, with metal inclusion sizes ranging from 0 to 4.0 mm. The S-parameters were recorded at the operating frequency of 11 GHz and plotted in Fig. 8. It is observed that the RF transparency decreases when the size of the metal inclusions increases as a result of the reflections off the metal meta-atoms. The effective permittivity of the meta-atoms is plotted in Fig. 9. As can be seen in the figure, the M2 achieves continuous permittivity values between 10 and 21.4. Because it renders meta-atoms extremely reflective and ideal for transparent metasurfaces, it is important to note that the maximum value of the metal inclusion is limited to 4 mm and not increased beyond that [8], [12]. Using both of the aforementioned methods, we can engineer low as well as high permittivity materials and have proposed a mechanism to devise values from 2.6 to 21.4 using the base material's permittivity of 10. In the next section, the idea of meta-atom design has been extended to develop highly transmitting MDCMs for beam steering applications.

IV. MDCM DESIGN STRATEGY

Instead of the much more time-consuming and computationally intensive process of first simulating all possible combinations of the meta-atoms by varying their physical geometric parameters [23], [35], we used a relatively straightforward method to design MDCM that relied on the effective characteristics of the meta-atoms. In order to do that, a reference database of transmission phases is taken into consideration for all-dielectric unit elements. Then the meta-atoms with equivalent phases can be substituted to develop the proposed MDCM. As a result, the first step is to create a reference database that covers the entire phase range from 0 to 360°, and can be used to compare the phase of proposed meta-atoms. For this purpose, a transmission phase ($\angle S_{21}$) database for ideal dielectrics was created. The overall procedures are further explained in the following subsections.

A. PHASE DELAY OF 2π FROM IDEAL DIELECTRIC

In our design strategy, we first use transmission line theory to predict transmission through ideal dielectric materials. To explain this further, consider an electric field propagation along a direction ($+z$-axis here). The transmission phase and magnitude between any two planes separated by a distance t in the direction of propagation can be analytically calculated using (12), and (13) derived via transmission line theory [36]. If the space between two virtual planes is occupied by a homogeneous dielectric of length h and air of length $(t\text{-}h)$, the total phase delay between these two planes is given by,

$$\varphi_{total} = \varphi_{dielectric} + \varphi_{air} \tag{12}$$

$$\varphi_{total} = \angle \frac{\tau_1 \tau_2 e^{-jk_1 h}}{1 + \rho_1 \rho_2 e^{-2jk_1 h}} + k_0(t-h) \tag{13}$$

where, τ_1 and τ_2 are intrinsic reflection coefficients of two mediums (air and dielectric), ρ_1 and ρ_2 intrinsic transmission coefficients of mediums. Further details on this phase delay between two imaginary planes have been reported in previous publications [36], [37] and are not repeated here for brevity.

Using (13), we predicted the phase and magnitude of the propagating electric field for various combinations of dielectric materials and their height, h. It is also considered that the spacing between two planes is 9.8 mm (or $t = 9.8$ mm). The height was varied from 1.4 mm to 9.8 mm while the permittivity was varied between 2.6 and 21.4. The maximum height value is set to a value that ensures a complete 2π phase shift for the given range of permittivity values. The magnitude and phase of the electric field are indicated in a color map plot against the two variables (permittivity and height of dielectric) in Fig. 10 (a) and (b). These two plots of ideal dielectrics are used as a reference database to select the appropriate heights and permittivity of meta-atoms (either M1 or M2) for attaining desired phase-shift through M1 and M2.

The selection of meta-atoms in a metasurface is guided by the desired tilt angle and progressive phase-delay gradient, as discussed in Section II. Considering the periodicity of

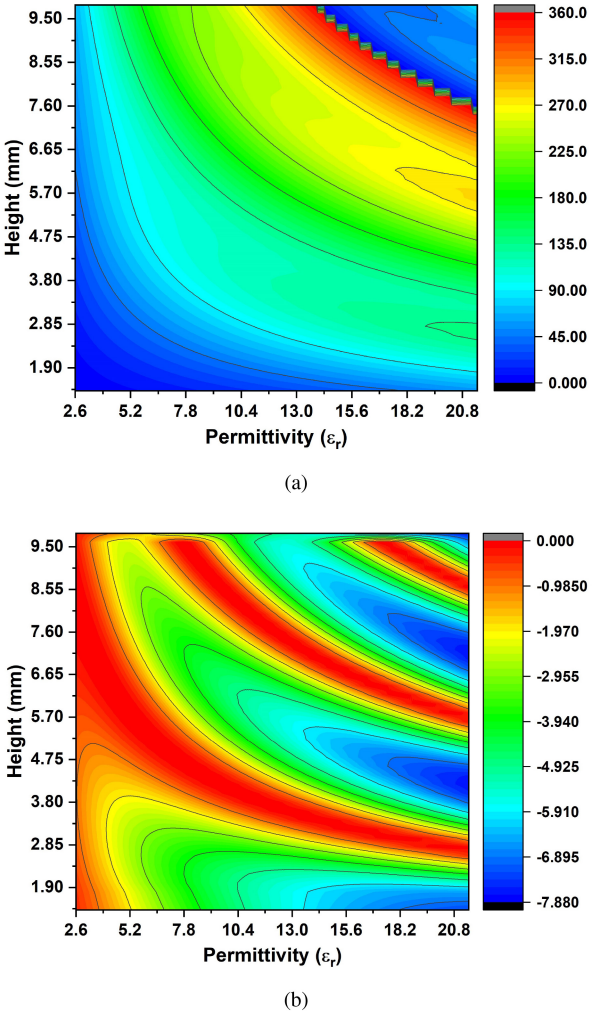

FIGURE 10. Database for transmission (a) phase and (b) magnitude of all-dielectric meta-atoms with the variations of height and permittivity.

meta-atom ($w = 7.8$ mm) and the desired tilt angle of each metasurface ($\delta = 26°$), the progressive phase delay of 45° is required between adjacent meta-atoms [38], [39]. From Fig. 10, we picked eight unique elements with a progressive phase delay of 45°. The geometric parameters (height and permittivity) of all eight elements of the all-dielectric surface are given in Table 2. It is to be mentioned here that while choosing elements with a progressive phase shift of 45°, there can be more than one element with different geometric parameters but identical phase shifts. In such cases, our selection is based on using the element having the least insertion loss while achieving the closest to the desired phase gradient. As an example, from Fig. 10, the elements with respective permittivities 5.7 and 8, and heights 9.8 and 7.6 return identical normalized phase of 180°. However, the loss of the former is −3.88 dB compared to that of −2.007 of the latter. Hence, the meta-atom with the lowest losses was considered. The eight ideal dielectric elements selected for the design of the beam-manipulating surface are not commercially available, so meta-atoms that have equivalent transmission and reflection characteristics to those of these eight dielectrics need to be artificially engineered.

B. META-ATOMS REPLACE IDEAL DIELECTRICS

The prime reason why metasurfaces with artificial dielectrics are superior to all-dielectric surfaces is that they have the ability to offer permittivity and phase values that cannot be offered by natural materials within the limited physical parameters. The incorporation of low-loss artificial dielectrics helps create highly transmitting metasurfaces within the limited permittivity and height range. The next step is to replace meta-atoms of equivalent transmission phases with those of specific all-dielectric unit elements to design MDCM with a high transmission magnitude while maintaining a low height profile. To convert all-dielectric elements to meta-atoms in the MDCMs, the height of all eight meta-atoms will remain the same as that of ideal dielectrics, but the effective permittivity will be achieved by replacing the ideal dielectric blocks with the meta-atoms with air or metal inclusion. If the permittivity value of a particular ideal dielectric element is lower than 10, then the corresponding meta-atom will have air inclusion, and if it exceeds 10 then a meta-atom with metal inclusion will be introduced.

This can be explained with one example. From Table 2, the first meta-atom of the ideal dielectric has a height of 1.4 mm and permittivity 2.6. From Fig. 7, it can be seen that by introducing perforation of 6.8 mm, the same effective permittivity can be achieved. So it can be assumed that an ideal dielectric unit element with permittivity of 2.6 and height of 1.4 mm will have the same reflection and transmission parameters as that of artificial dielectric with host permittivity of 10 and 6.8 mm cubical air inclusion. It was verified by simulating both meta-atoms in CST Microwave Studio. Likewise, other dielectric elements in Table 2 were replaced by meta-atoms. The corresponding heights for both types of meta-atom were the same and the effective permittivity of the ideal dielectric meta-atom was achieved by finding the right inclusion size from Fig. 7 and Fig. 9. This design procedure, thus, did not involve any parametric sweep and hence synthetic metasurface with artificial materials can easily be coined using this technique.

Another way to design MDCM with greater flexibility is to select all height and permittivity values from the all-dielectric database that have identical transmission phases with the progressive phase delay of 45°. As a result, multiple meta-atoms will have identical $\angle S_{21}$ values, and one with the highest transmission can be chosen to incorporate in MDCM. For example, consider three meta-atoms with respective heights of 7.8 mm, 8.8 mm, and 9.6 mm, and perforation sizes of 1.6 mm, 2.8 mm, and 4.4 mm. They have almost identical $\angle S_{21}$ of 1.5°, 0.74° and 1.13° and their respective insertion losses are 2.4 dB, 0.74 dB and 4.6 dB. Hence, the meta-atom with a height of 8.8 mm and perforation size of 2.8 mm will be used to develop MDCM, as it has the lowest insertion loss.

TABLE 2. Dimensions and transmission phase for ideal dielectric elements and proposed meta-atoms to create MDCMs.

Meta-atoms	Normalized Phase (°)	Height (mm)	Ideal Dielectric		Meta-atoms	
			Relative Permittivity	Simulated Phase (°)	Perforation size, b or metal size, d (mm)	Simulated Phase (°)
1	0	1.4	2.6	34	b = 6.8	34
2	45	6.2	2.6	78	b = 6.8	78
3	90	6.2	4.9	124	b = 5.4	124
4	135	9.7	4.5	169	b = 5.7	169
5	180	9.8	5.7	-147	b = 4.9	-147
6	225	9.6	8.1	-102	b = 3.1	-102
7	270	6.2	17.6	-57	d = 3.4	-57
8	315	9.8	12.2	-12	d = 2.0	-12

This is critical for AM process as different models of 3D printers have variable design dimension constraints, and a set of meta-atoms with desirable inclusion sizes can be chosen according to the printer's limitation for MDCM design. Moreover, the freedom to choose from multiple meta-atoms with identical transmission phases allows selecting the desired number of meta-atoms with air or metal inclusions because phase overlap exists for both inclusion types. Meta-atoms with air inclusions offer a normalized phase range between 0° to 258.58° and those with metal inclusions have a normalized phase range from 77.1° to 331.7°. Hence, the phase range of 77.1° to 258.58° overlaps, and either meta-atom (with air or metal inclusion) can be selected for MDCM design. This has been depicted as transmission phase vs. insertion loss in Fig. 11 (a) and (b) in the form of a database of precomputed values.

C. ARRANGEMENT OF META-ATOMS

The chosen eight meta-atoms are then strategically arranged with a phase delay gradient to form MDCM, which has a constant phase in the y-axis and a progressive phase in the x-axis. It implies that meta-atoms will be repeated in the y-axis and will have increasing phase delay in the x-axis. A total of twenty-one meta-atoms were arrayed to form the metasurface of size 163.8 mm ($6\lambda_0$). In this way, low-cost 3D printable synthetic MDCM can be realized using filaments with thermoplastics, polymers, metallic, and ceramic inclusions, as shown in Fig. 12. Metal composites can be printed using Markforged printers, and dielectrics can be printed using polymer printers.

V. RESULTS AND DISCUSSION

To demonstrate the efficacy of the MDCM pair, a beam-steering antenna is developed to steer the broadside beam of a patch array antenna. The overall antenna configuration is shown in Fig. 13. A classical patch array of diameter 163.8 mm ($6\lambda_0$) is used as a primary feed. The array comprises 90 patches, each having lateral dimensions of 7.96mm×6.96mm. The basic configuration of the patch array with MDCM pair is shown in Fig. 13. The array has an extended ground plane and Rogers Ultralam 2000 ($\epsilon_r = 2.5$) substrate of thickness 1.59 mm. The MDCM pair is suspended at 13.8 mm ($\approx 0.5\lambda_0$) above the feed, and the subwavelength gap between the two MDCMs is 4 mm. It is important to note that such air spacings affect the overall antenna beam-steering performance and should be optimized at the design level. A detailed discussion is already given in the reported article [23] and is not repeated here for brevity. The relative angular positions of MDCMs can dynamically define the beam directions over a large conical space in the upper hemisphere. Controls of azimuth and elevation angles for two different beam steering configurations, namely elevation and azimuth scanning (Case I) and elevation scanning only (Case II), have been demonstrated in the following sub-sections. These configurations are simulated with the full-wave transient solver in CST Microwave Studio. The predicted results are then compared with the analytical results to validate the beam steering method using the proposed synthetic MDCMs.

A. CASE I: SIMULTANEOUS BEAM-STEERING IN THE ELEVATION AND AZIMUTH PLANES

The first configuration demonstrates simultaneous variation in azimuth and elevation angle, for which, MDCM-1 is fixed, and MDCM-2 is rotated in the counter-clockwise direction in steps of 30°, i.e., $\alpha_1 = 0°$ and $\alpha_2 = 30°, 60°, \ldots, 180°$. This results in six different orientations of MDCM-2, and the beam peak has a distinct azimuth and elevation angle for each orientation. The radiation patterns for all six orientations are predicted through a full-wave simulation environment. All the elevation cuts, taken at azimuth angles, containing beam peaks are plotted in Fig. 14.

The elevation angle is maximum, i.e., $\theta = \theta_{max} = 55°$ when $\alpha_1 = 0°$ and $\alpha_2 = 30°$. With the stepped increase in α_2 from 30° to 180°, the beam simultaneously moves in the azimuth and elevation planes and ends up in a broadside direction. A comparison between theoretically estimated and predicted values through full-wave EM simulations of the elevation angles of the beam peaks is given in Table 3.

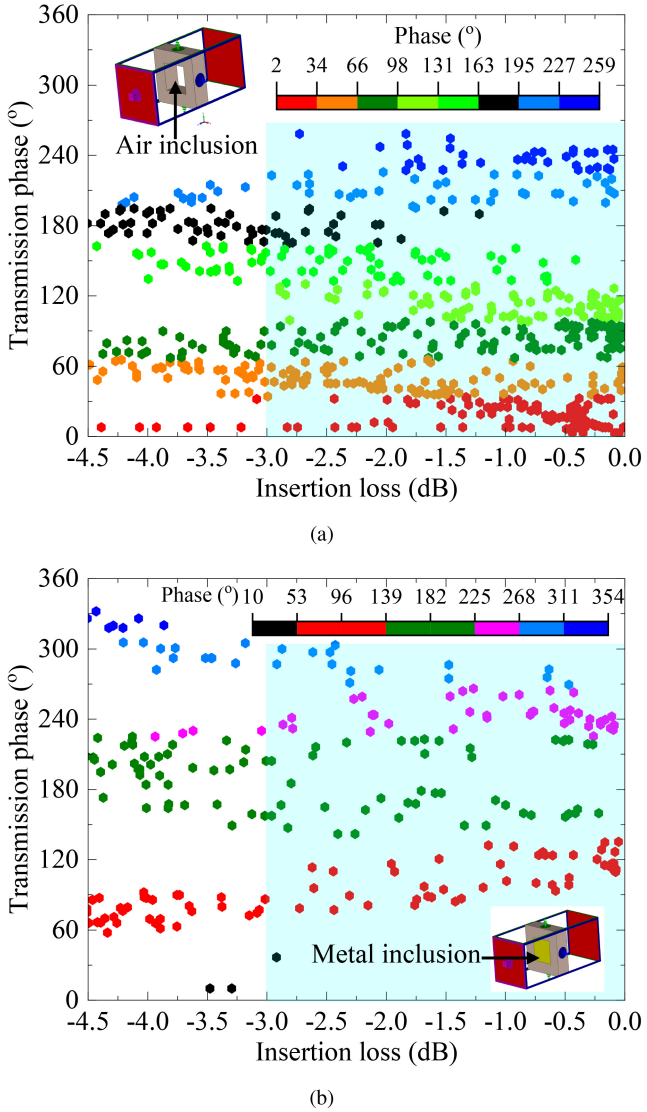

FIGURE 11. Transmission phase achieved by meta-atoms with varying dielectric heights from 1.6 mm to 9.8 mm. Meta-atoms with (a) air and (b) metal inclusions.

TABLE 3. Comparison of theoretically estimated and numerically predicted beam positions for Case I.

MDCMs Position		Estimated Direction	Simulated Direction	Difference
$\alpha_1(^\circ)$	$\alpha_2(^\circ)$	$\theta_E(^\circ)$	$\theta_S(^\circ)$	$\lvert\theta_E - \theta_S\rvert(^\circ)$
0	30	56	54	2
0	60	44	46	2
0	90	36	34	2
0	120	26	25	1
0	150	12	12	0
0	180	0	0	0

The precise angular positions of the beam peaks are estimated analytically using (10) and (11). Whereas, for a special condition of $\delta_1 = \delta_2$, the azimuth angle (ϕ) of the beam

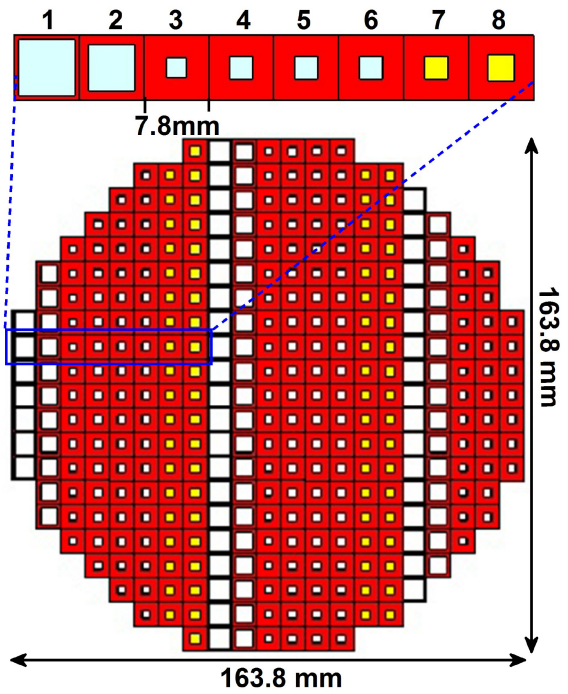

FIGURE 12. Front view of 3D printable synthetic MDCM model with a set of eight meta-atoms with varying geometries magnified in the inset.

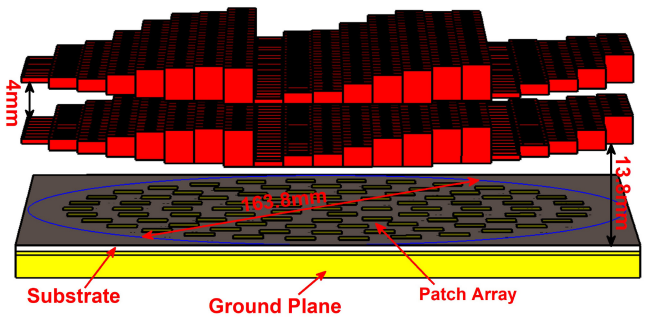

FIGURE 13. A beam-steering antenna using a pair of MDCMs. A patch array antenna is used as a primary feed source.

peaks can be calculated using (14) [27].

$$\phi = \left(\frac{\alpha_1 + \alpha_2}{2}\right) \tag{14}$$

The values of azimuth and elevation angles for all six orientations of the MDCM pair are given in the legend of Fig. 14. The elevation angle (θ) is the beam peak's position on the figure's horizontal axis. The maximum peak directivity of 19.9 dB is achieved when the MDCM pair is oriented 180° apart, i.e., $\alpha_1 = 0°$ and $\alpha_2 = 180°$ and the beam points in the broadside direction. The minimum peak directivity of 17 dBi is achieved when the beam is scanned furthest in the elevation for $\alpha_1 = 0°$ and $\alpha_2 = 0°$. Such phenomena are very common in the near-field meta-steering antenna systems [3], [21], [23].

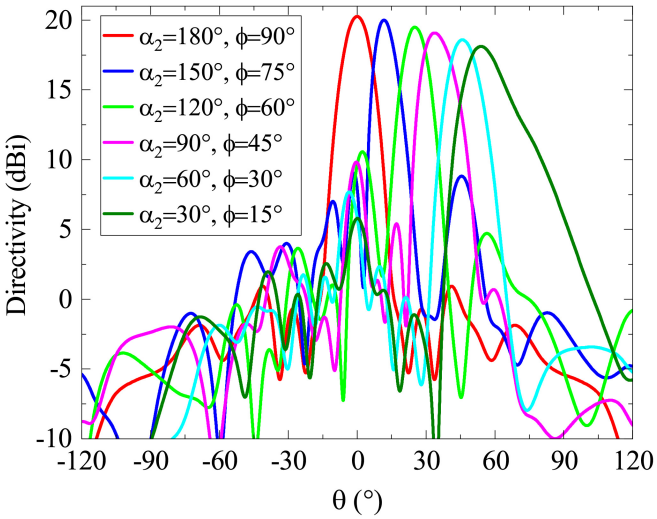

FIGURE 14. Predicted radiation pattern cuts for the case when MDCM-1 is fixed at $\alpha_2 = 0°$ and MDCM-2 is rotated from $\alpha_2 = 30°$ to $180°$ in steps of $30°$.

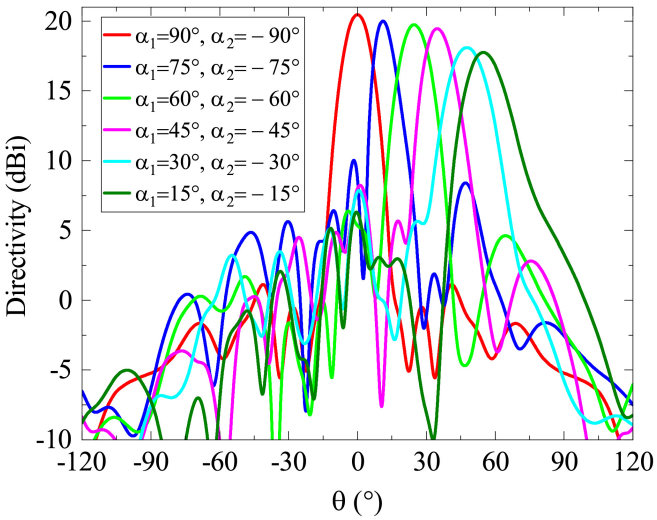

FIGURE 15. Predicted radiation pattern cuts taken at $\phi = 0°$ for the case when both MDCM-1 and MDCM-2 are rotated equally in the opposite directions (i.e., $\alpha_2 = -\alpha_1$).

B. CASE II: BEAM-STEERING IN THE ELEVATION PLANE ONLY

The two MDCMs are rotated equally in opposite directions for sole elevation angle variation without affecting the azimuth angle. Similar to the prior instance, simulations for six alternative orientations of the MDCM pair are used to confirm the variance in elevation angles. MDCM-1 is rotated clockwise by 15° from $\alpha_1 = 15°$ to 90°, whereas MDCM-2 is rotated anticlockwise by the same steps, from $\alpha_2 = -15°$ to $-90°$.

The elevation cuts for all orientations of the MDCM pair containing the beam peak (taken at $\phi = 0°$) are plotted in Fig. 15. The beam peak is in the broadside direction when $\alpha_1 = 90°$ and $\alpha_2 = -90°$ and it gradually reduces with the increase in elevation angle. Like the previous case of configurations, the highest peak directivity of 18.9 dBi is exhibited in the broadside direction, and the lowest directivity of 16.1 dBi is observed for $\alpha_1 = 15°$ and $\alpha_2 = -15°$ when the beam points to the largest elevation angle of 57°. The orientation of the MDCMs (relative angular positions) and a comparison between beam peaks estimated using (10) and (11) and predicted by the simulations are given in Table 5. They agree well; the difference is not more than 5°.

TABLE 4. Comparison of theoretically estimated and numerically predicted beam positions for Case II.

MDCMs Position		Estimated Direction	Simulated Direction	Difference
$\alpha_1(°)$	$\alpha_2(°)$	$\theta_E(°)$	$\theta_S(°)$	$\lvert\theta_E - \theta_S\rvert(°)$
15	-15	57	55	2
30	-30	43	48	5
45	-45	35	36	1
60	-60	24	25	1
95	-75	13	11	2
90	-90	0	0	0

Table 5 compares the key features of the proposed antenna with state-of-the-art technologies to assess the MDCM's efficacy. Its footprint is smaller, and its design is straightforward. Table 5 demonstrates that the physical and electrical performance of the patch array with MDCM is comparable and promising. It has similar directivity/gain, better scanning capability and aperture efficiency. The proposed 3D printed technology is an alternative to the PCB technology with rapid prototyping, lower cost and little to no human intervention. In comparison to alternative approaches, such as an all-metal transmitarray [22] or a beam-steering antenna with a metal-only phase gradient metasurface [23], the antenna profile is also significantly reduced. Additionally, the MDCM only needs one filament to build, in contrast to the counter design's requirement for at least four different 3D filaments and extremely precise micro-milling methods [21].

VI. CONCLUSION

Low-cost metal-dielectric composite metasurfaces (MDCMs) have been presented for beam steering applications of a fixed-beam static base antenna. The MDCMs can be realized using filaments with thermoplastics, polymers, ceramics, and metallic composites, where phase transition through MDCMs is locally controlled by varying permittivity values from 2.6 to 21.4. The nearly continuous permittivity range is achieved with synthetic MDCM, which cannot be realized through metasurfaces developed using commercial off-the-shelf standard materials. Such MDCM can be fabricated in a single step, eliminating the tedious machining or bonding typically required in multilayered thin metasurfaces. It should be noted that the properties of 3D printed structures may differ from

TABLE 5. Performance comparison with the state-of-the-art published works.

Ref.	Operating Frequency (GHz)	Feed Antenna & Steering Method	MS/PT Types & Technology	MS/PT Thickness (λ_0)	Peak Gain (dBi)	Maximum Steering El/Az (°)	MS/PT Aperture Size (λ_0)	Max. Aperture Efficiency (%)	Antenna Profile (Including Feed) (λ_0)
This Work	**11.0**	**Patch Array NFMS-RP**	**Composite, 3D Printed Single Filament**	**0.36**	**19.9***	**±57/360**	**6.0**	**21.56**	**1.38**
[3] IEEE TAP	11.0	RCA NFMS-RP	Composite, PCB	0.12	19.4	±46/360	6.0	24.41	1.3
[20] IEEE Access	30.0	WR28 NFMS-RP	Dielectric, 3D Printed Single Filament	3.19	16.0	±39/360	6.0	11.21	8.1
[28] IEEE Access	11.0	Horn NFMS-RP	Dielectric, 3D Printed Single Filament	1.76	15.4	±36/360	4.2	19.7	6.3
[21] IEEE TAP	34.5	Horn NFMS-RP	Dielectric, 3D Printed Multiple Filaments	0.51	21.6	±54/360	5.9	42.0	10.2
[22] IEEE TAP	9.375	Horn TA-PR	All-Metal, Laser-Cut	0.94	–	±20/360	8.0	–	15.3
[23] IEEE TAP	12.5	Horn NFMS-RP	Metal, Laser-Cut	0.80	16.0	±42/360	6.0	11.21	4.9

'–' data is unavailable, NFMS – Near-Field Meta-Steering, RP – Risley Prism, RCA – Resonant Cavity Antenna, PCB – Printed Circuit Board, Directivity, MS/PT – Metasurface/Phase Transformer, El/Az - Elevation/Azimuth, IEEE TAP – IEEE Transactions on Antennas and Propagation.

the bulk materials' properties (i.e., reduced relative permittivity, increased losses etc.), which could be considered during the 3D printing stage. Full-wave numerical simulation results show that a patch array antenna's beam can be steered at a large apex angle of 114° with a maximum directivity of 19.9 dBi and a worst-case scanning loss of only 2.9 dB using a pair of MDCMs.

REFERENCES

[1] L. Zhang, S. Mei, K. Huang, and C. W. Qiu, "Advances in full control of electromagnetic waves with metasurfaces," *Adv. Opt. Mater.*, vol. 4, no. 6, pp. 818–833, 2016.

[2] C. Huang, C. Zhang, J. Yang, B. Sun, B. Zhao, and X. Luo, "Reconfigurable metasurface for multifunctional control of electromagnetic waves," *Adv. Opt. Mater.*, vol. 5, no. 22, 2017, Art. no. 1700485.

[3] M. U. Afzal and K. P. Esselle, "Steering the beam of medium-to-high gain antennas using near-field phase transformation," *IEEE Trans. Antennas Propag.*, vol. 65, no. 4, pp. 1680–1690, Apr. 2017.

[4] V. G. Ataloglou et al., "Static and reconfigurable Huygens' metasurfaces: Use in antenna beamforming and beam steering," *IEEE Antennas Propag. Mag.*, vol. 64, no. 4, pp. 73–84, Aug. 2022.

[5] P. Ikonen et al., *Artificial Electromagnetic Composite Structures in Selected Microwave Applications*, Helsinki Univ. Technol., Helsinki, Finland, 2007.

[6] A. Sihvola, "Metamaterials in electromagnetics," *Metamaterials*, vol. 1, no. 1, pp. 2–11, 2007.

[7] X. Luo, "Subwavelength artificial structures: Opening a new era for engineering optics," *Adv. Mater.*, vol. 31, no. 4, 2019, Art. no. 1804680.

[8] R. K. Arya, S. Pandey, and R. Mittra, "Flat lens design using artificially engineered materials," *Prog. Electromagn. Res. C*, vol. 64, pp. 71–78, May 2016.

[9] G.-L. Huang, S.-G. Zhou, C.-Y.-D. Sim, T.-H. Chio, and T. Yuan, "Lightweight perforated waveguide structure realized by 3-D printing for RF applications," *IEEE Trans. Antennas Propag.*, vol. 65, no. 8, pp. 3897–3904, Aug. 2017.

[10] T. Hayat, M. U. Afzal, F. Ahmed, S. Zhang, K. P. Esselle, and Y. Vardaxoglou, "Low-cost ultrawideband high-gain compact resonant cavity antenna," *IEEE Antennas Wireless Propag. Lett.*, vol. 19, no. 7, pp. 1271–1275, Jul. 2020.

[11] T. Hayat, M. U. Afzal, F. Ahmed, and K. P. Esselle, "Design and performance comparison of compact resonant cavity antennas using Customized 3D printing techniques," in *Proc. 16th Eur. Conf. Antennas Propag. (EuCAP)*, 2022, pp. 1–5.

[12] N. Gagnon, A. Petosa, and D. A. Mcnamara, "Thin microwave quasi-transparent phase-shifting surface (PSS)," *IEEE Trans. Antennas Propag.*, vol. 58, no. 4, pp. 1193–1201, Apr. 2010.

[13] H. Lipson and M. Kurman, *Fabricated: The New World of 3D Printing*. Hoboken, NJ, USA: Wiley, 2013.

[14] H. Giddens, A. S. Andy, and Y. Hao, "Multimaterial 3-D printed compressed Luneburg lens for mm-Wave beam steering," *IEEE Antennas Wireless Propag. Lett.*, vol. 20, no. 11, pp. 2166–2170, Nov. 2021.

[15] Y. Cheng, X. Wang, and Y. Dong, "Broadband dual-polarized metal lens with theoretically arbitrarily variable focal diameter ratio using 3-D printing technology," *IEEE Trans. Antennas Propag.*, vol. 70, no. 9, pp. 7774–7785, Sep. 2022.

[16] F.-E. Zerrad et al., "Symmetrical and asymmetrical breast phantoms with 3D-printed anatomical structure for microwave imaging of breast cancer," *IEEE Access*, vol. 10, pp. 96896–96908, 2022.

[17] "PREPERM—3D ABS1000 filament 1.75mm 750g-PREPERM—Webshop." Accessed: May 16, 2023. [Online]. Available: https://www.avient.com/resources/technical-data-sheets:PrepermABS1000

[18] M. T. Sullivan. "Synopsis of risley prism beam pointer." 2006. [Online]. Available: http://www.coastalopt.com/

[19] P. Church, J. Matheson, X. Cao, and G. Roy, "Evaluation of a steerable 3D laser scanner using a double Risley prism pair," in *Proc. Degraded Environ. Sens. Process. Display*, vol. 10197, pp. 203–211, 2017,

[20] M. U. Afzal, L. Matekovits, K. P. Esselle, and A. Lalbakhsh, "Beam-scanning antenna based on near-electric field phase transformation and refraction of electromagnetic wave through dielectric structures," *IEEE Access*, vol. 8, pp. 199242–199253, 2020.

[21] A. A. Baba, R. M. Hashmi, M. Attygalle, K. P. Esselle, and D. Borg, "Ultrawideband beam steering at mm-Wave frequency with planar dielectric phase transformers," *IEEE Trans. Antennas Propag.*, vol. 70, no. 3, pp. 1719–1728, Mar. 2022.

[22] X. Zhao et al., "All-metal beam steering lens antenna for high power microwave applications," *IEEE Trans. Antennas Propag.*, vol. 65, no. 12, pp. 7340–7344, Dec. 2017.
[23] F. Ahmed, M. U. Afzal, T. Hayat, K. P. Esselle, and D. N. Thalakotuna, "A near-field meta-steering antenna system with fully metallic metasurfaces," *IEEE Trans. Antennas Propag.*, vol. 70, no. 11, pp. 10062–10075, Nov. 2022.
[24] F. Ahmed, M. U. Afzal, K. Singh, T. Hayat, and K. P. Esselle, "Highly transparent fully metallic 1-bit coding metasurfaces for near-field transformation," in *Proc. 16th Eur. Conf. Antennas Propag. (EuCAP)*, 2022, pp. 1–4.
[25] J. Melendro-Jimenez, P. Sanchez-Olivares, A. Tamayo-Dominguez, X. Sun, and J. M. Fernandez-Gonzalez, "3D printed directive beam-steering antenna based on gradient index flat lens with an integrated polarizer for dual circular polarization at W-band," *IEEE Trans. Antennas Propag.*, vol. 71, no. 1, pp. 1059–1064, Jan. 2023.
[26] Z. Wei, Y. Cao, X. Su, Z. Gong, Y. Long, and H. Li, "Highly efficient beam steering with a transparent metasurface," *Opt. Exp.*, vol. 21, no. 9, 2013, Art. no. 10739.
[27] J. Wang and Y. Ramhat-Samii, "Phase method: A more precise beam steering model for phase-delay metasurface based Risley antenna," in *Proc. URSI Int. Symp. Electromagn. Theory (EMTS)*, 2019, pp. 1–4.
[28] T. Hayat, M. U. Afzal, F. Ahmed, S. Zhang, K. P. Esselle, and J. Vardaxoglou, "The use of a pair of 3D-printed near field super-structures to steer an antenna beam in elevation and azimuth," *IEEE Access*, vol. 9, pp. 153995–154010, 2021.
[29] C. R. Simovski, P. A. Belov, and S. He, "Backward wave region and negative material parameters of a structure formed by lattices of wires and split-ring resonators," *IEEE Trans. Antennas Propag.*, vol. 51, no. 10, pp. 2582–2591, Oct. 2003.
[30] P. Markos and C. Soukoulis, "Transmission properties and effective electromagnetic parameters of double negative metamaterials," *Opt. Exp.*, vol. 11, no. 7, p. 649, 2003.
[31] X. Chen, T. M. Grzegorczyk, B.-I. Wu, J. Pacheco, and J. A. Kong, "Robust method to retrieve the constitutive effective parameters of metamaterials," *Phys. Rev. E, Stat. Phys. Plasmas Fluids Relat. Interdiscip. Top.*, vol. 70, Jul. 2004, Art. no. 16608.
[32] D. R. Smith, D. C. Vier, T. Koschny, and C. M. Soukoulis, "Electromagnetic parameter retrieval from inhomogeneous metamaterials," *Phys. Rev. E, Stat. Phys. Plasmas Fluids Relat. Interdiscip. Top.*, vol. 71, no. 3, 2005, Art. no. 36617.
[33] A. B. Numan and M. S. Sharawi, "Extraction of material parameters for metamaterials using a full-wave simulator [education column]," *IEEE Antennas Propag. Mag.*, vol. 55, no. 5, pp. 202–211, Oct. 2013.
[34] T. Hayat, M. U. Afzal, A. Lalbakhsh, and K. P. Esselle, "Additively manufactured perforated superstrate to improve directive radiation characteristics of electromagnetic source," *IEEE Access*, vol. 7, pp. 153445–153452, 2019.
[35] N. Gagnon, *Phase Shifting Surface (PSS) and Phase and Amplitude Shifting Surface (PASS) for Microwave Applications*, Univ. Ottawa, Ottawa, ON, Canada, 2011.
[36] S. J. Orfanidis, *Electromagnetic Waves and Antennas*. Piscataway, NJ, USA: Rutgers Univ., 2008.
[37] M. U. Afzal, K. P. Esselle, and B. A. Zeb, "Dielectric phase-correcting structures for electromagnetic band gap resonator antennas," *IEEE Trans. Antennas Propag.*, vol. 63, no. 8, pp. 3390–3399, Aug. 2015.
[38] X. Fu, F. Yang, C. Liu, X. Wu, and T. J. Cui, "Terahertz beam steering technologies: From phased arrays to field-programmable metasurfaces," *Adv. Opt. Mater.*, vol. 8, no. 3, 2020, Art. no. 1900628.
[39] Y. H. Lv, X. Ding, B.-Z. Wang, and D. E. Anagnostou, "Scanning range expansion of planar phased arrays using metasurfaces," *IEEE Trans. Antennas Propag.*, vol. 68, no. 3, pp. 1402–1410, Mar. 2020.

FOEZ AHMED (Member, IEEE) received the B.Sc. (Hons.) and M.Sc. degrees in information and communication engineering from the University of Rajshahi (RU), Rajshahi, Bangladesh, in 2007 and 2009, respectively, and the M.Eng. degree in electrical and computer engineering from the South China University of Technology (SCUT), Guangzhou, China, in 2013. He is currently pursuing the Ph.D. degree with the School of Electrical and Data Engineering, University of Technology Sydney (UTS), Sydney, NSW, Australia.

From 2012 to 2014, he was a Lecturer with the Department of Information and Communication Engineering, RU, where he has been an Assistant Professor since 2014 (now on study leave). He was also a Lecturer with the Northern University of Bangladesh, Dhaka, Bangladesh, from 2008 to 2009, and King Khalid University, Abha, Saudi Arabia, from 2009 to 2011. His current research interests include high-gain antennas, SATCOM antennas, metasurfaces, frequency-selective surfaces, and far-field pattern synthesis using near-field phase transformation.

Mr. Ahmed was a recipient of several prestigious awards and scholarships, including the Commonwealth-Funded International Research Training Program Scholarship, the Post Thesis Scholarship, the International Research Scholarship (IRS) and the Faculty of Engineering and Information Technology (FEIT) Scholarship from UTS; the Gold Medal from RU, the Chinese Government Scholarship; the Academic Achievement Award, and the Excellency Award from SCUT, China. On top of that, he also received faculty-wide highly competitive research grants and travel funds, including the Vice-Chancellor's Conference Fund, the Faculty Conference Fund, the School Travel Fund from UTS and the Postgraduate Research Fund from Macquarie University, Sydney, Australia.

TOUSEEF HAYAT (Graduate Student Member, IEEE) received the B.S. degree in telecommunication engineering from the University of Engineering and Technology Taxila, Taxila, Pakistan, the M.S. degree (Hons.) from the National University of Sciences and Technology, Islamabad, Pakistan, and the Master of Research (MRes) degree (Hons.) in electronics engineering from Macquarie University, Australia, in 2018, where he is currently pursuing the Ph.D. degree.

His research interests include electromagnetic-bandgap resonant antennas, additive manufacturing of microwave components, phase- and amplitude-transforming metasurfaces, and dielectric characterization. He received several prestigious awards, including the International Research Training Program Scholarship for the MRes and the International Macquarie University Research Excellence Scholarship for his Ph.D. degree.

MUHAMMAD U. AFZAL (Senior Member, IEEE) received the bachelor's degree (Hons.) in electronics engineering and the master's degree in computational science and engineering from the National University of Sciences and Technology (NUST), Islamabad, in 2009 and 2011, respectively, and the Ph.D. degree in electronics engineering from Macquarie University, Australia, in 2017.

In 2010, he started his professional career as a Laboratory Engineer with the Research Institute for Microwave and Millimetre-Wave Studies, NUST, where he was promoted as a Lecturer, in 2012, which he continued until February 2013. After his Ph.D. degree, he was offered a postdoctorate for three years on a project funded by the Australian Research Council (ARC) through the Discovery Grant Scheme at Macquarie University. He is currently a Research Fellow working with the University of Technology Sydney. He developed the concept of near-field phase transformation during his doctorate research, which was demonstrated to enhance the directivity of low-gain aperture antennas in IEEE TRANSACTIONS ON ANTENNAS AND PROPAGATION paper titled "Dielectric phase-correcting structures for electromagnetic band-gap resonator antennas." He is the co-inventor of efficient antenna beam-steering technology referred to as near-field meta-steering. This technology received the "Highly Commended" Certificate in the five future-shaping research priorities category in the 2017 Academic Staff Awards at Macquarie University. To commercialize the outcomes of his research, he led a team of colleagues in a CSIRO sponsored ON Prime 2, in 2017, a pre-accelerator program designed to commercialize outcomes of academic research in Australia. Apart from the project-specific research, he co-supervised one Ph.D., three master's of research, and several undergraduate thesis students at Macquarie University. He is also working on the development of satellite-terminal antenna technology. His research interests include electromagnetic phase-shifting structures, frequency selective surfaces, and similar metamaterials for microwave and millimeter-wave antenna applications.

Dr. Afzal has received several awards and scholarships, including a merit-based scholarship in six out of eight semesters during the undergraduate degree, a scholarship of complete fee waiver during the postgraduate degree, and the International Macquarie Research Excellence Scholarship toward doctorate study from Macquarie University. He received the Competitive Travel Grant, in 2015, to present his research work at a flagship conference under the Antennas and Propagation Society in Vancouver, Canada. He assisted in preparing several grant applications, including a successful ARC Discovery Grant, in 2018. He was third CI in a team of five who received a grant of more than $20K from the German Academic Exchange Service in a funding scheme "Australia–Germany Joint Research Co-Operation Scheme."

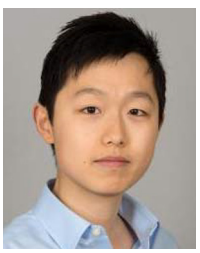

SHIYU ZHANG received the M.Sc. degree from The University of Manchester, Manchester, U.K., in 2010, and the Ph.D. degree from Loughborough University, Loughborough, U.K., in 2014.

Following graduation, he worked as a Research Associate with Loughborough University, where he is currently with the Wolfson School of Mechanical, Electrical, and Manufacturing Engineering. His current research interests include engineered electromagnetic structures (metamaterials, metasurfaces, and frequency selective surfaces), antennas and RF circuit components, additive manufacturing (3-D-printing), and wearable antennas and electronic systems.

Dr. Zhang received the EPSRC Doctoral Prize Research Fellowship in 2015, and he was the recipient of the First Runner-Up of the 2013 Loughborough Antennas and Propagation Conference (LAPC) IET Best Student Paper Award. He served as the Technical Program Committee Member for the LAPC in 2017 and 2018.

KARU P. ESSELLE (Fellow, IEEE) received the B.Sc. degree (First-Class Hons.) in electronic and telecommunication engineering from the University of Moratuwa, Sri Lanka, and the M.A.Sc. and Ph.D. degrees (with near-perfect GPA) in electrical engineering from the University of Ottawa, Canada.

He is the Distinguished Professor of Electromagnetic and Antenna Engineering with the University of Technology Sydney and a Visiting Professor with Macquarie University, Sydney. He is a Fellow of the Royal Society of New South Wales and Engineers Australia. Previously, he was the Director of WiMed Research Centre and an Associate Dean—Higher Degree Research of the Division of Information and Communication Sciences and directed the Centre for Collaboration in Electromagnetic and Antenna Engineering with Macquarie University. He has also served as a member of the Dean's Advisory Council and the Division Executive and as the Head of the Department several times. He is the Director of Innovations for Humanity Pty Ltd. He has provided expert assistance to more than a dozen companies, including Intel, Hewlett Packard Laboratory, USA, Cisco Systems, USA, Audacy, USA, Cochlear, Optus, ResMed, and Katherine-Werke, Germany. His team designed the high-gain antenna system for the world's first entirely Ka-band CubeSat made by Audacy, and launched to space by SpaceX in December 2018. This is believed to be the first Australian-designed high-gain antenna system launched to space, since CSIRO-designed antennas in Australia's own FedSat launched in 2002. He was in the College of Expert Reviewers of the European Science Foundation from 2019 to 2022 and he has been invited to serve as an international expert/research grant assessor by several other research funding bodies as well, including the European Research Council and funding agencies in Norway, Belgium, the Netherlands, Canada, Finland, Hong Kong, Georgia, South Africa, and Chile. He has been invited by Vice-Chancellors of Australian and overseas universities to assess applications for promotion to professorial levels. He has authored over 650 research publications and his papers have been cited ∼12 500 times. In 2021, his publications received over 1400 citations. His h-index is 53 and i-10 is 212. Since 2002, his research team has been involved with research grants, contracts, and Ph.D. scholarships worth over $22 Million, including 15 Australian Research Council grants, without counting the 245 million-dollar SmartSat Corporative Research Centre, which started in 2019. His research has been supported by many national and international organizations, including Australian Research Council, Intel, U.S. Air Force, Cisco Systems, Hewlett-Packard, Australian Department of Defence, Australian Department of Industry, NSW Chief Scientist & Engineer Office, and German and Indian governments.

Dr. Esselle's most recent awards include the Top Space Award in Australia—the "Winner of Winners" Excellence Award—as well as the Academic of Year Award at the 2022 Australian Space Awards, both the most prestigious Excellence Award and the Academic of the Year Award at 2021 Australian Defence Industry Awards, the Finalist for 2021 Australian national Eureka Prize for Outstanding Mentor of Young Researchers, Runner-Up to the same prize in 2020, the 2019 Motohisa Kanda Award (from IEEE USA) for the most cited paper in IEEE TRANSACTIONS ON ELECTROMAGNETIC COMPATIBILITY in the past five years, the 2021 IEEE Region 10 (Asia–Pacific) Outstanding Volunteer Award, and the 2020 IEEE NSW Outstanding Volunteer Award. According to the Special Report on Research published by The Australian National Newspaper, he is the 2019 National Research Field Leader in Australia in both Microelectronics and Electromagnetism fields. Previously, he received the 2019 Macquarie University Research Excellence Award for Innovative Technologies, the 2019 ARC Discovery International Award, the 2017 Excellence in Research Award from the Faculty of Science and Engineering, the 2017 Engineering Excellence Award for Best Innovation, the 2017 Highly Commended Research Excellence Award from Macquarie University, the 2017 Certificate of Recognition from IEEE Region 10, the 2016 and 2012 Engineering Excellence Awards for Best Published Paper from IESL NSW Chapter, the 2011 Outstanding Branch Counsellor Award from IEEE headquarters, USA, the 2009 Vice Chancellor's Award for Excellence in Higher Degree Research Supervision, and the 2004 Innovation Award for Best Invention Disclosure. His mentees have been awarded many fellowships, awards, and prizes for their research achievements. Fifty-eight international experts who examined the theses of his Ph.D. graduates ranked them in the top 5% or 10%. Two of his students were awarded Ph.D. with the highest honor at Macquarie University—the

Vice Chancellor's Commendation, and one received University Medal for Master of Research. In addition to the IEEE Kanda Award mentioned above, several of his papers have been among the most cited or most downloaded. For example, one he coauthored on All-metal Wideband Metasurface on Scientific Reports in May 2021 was selected by Web of Science-Clarivate as both a Highly cited paper (top 1% in the academic field of Engineering) as well as a Hot paper (to 1% in Engineering). He is in world's top 100 000 most-cited scientists list by Mendeley Data. From 2018 to 2020, he chaired the prestigious Distinguished Lecturer Program Committee of the IEEE Antennas and Propagation (AP) Society—the premier global learned society dedicated for antennas and propagation—which has close to 10 000 members worldwide. After two stages in the selection process, he was also selected by this Society as one of two candidates in the ballot for 2019 President of the Society. Only three people from Asia or Pacific apparently have received this honor in the 68-year history of this Society. He is also one of the three Distinguished Lecturers (DL) selected by the Society in 2016. He is the only Australian to chair the AP DL Program ever, the only Australian AP DL in almost two decades, and second Australian AP DL ever (after UTS Distinguished Visiting Professor Trevor Bird). He has served the IEEE AP Society Administrative Committee in several elected or ex-officio positions 2015–2020. He is also the Chair of the Board of Management of Australian Antenna Measurement Facility, and was the elected Chair of both IEEE New South Wales (NSW), and IEEE NSW AP/MTT Chapter, in 2016 and 2017. He has also been invited to assess grant applications submitted to Australia's most prestigious schemes, such as Australian Federation Fellowships and Australian Laureate Fellowships. In addition to the large number of invited conference speeches he has given, he has been an invited plenary/extended/keynote/distinguished speaker of several IEEE and other venues over 30 times, including EuCAP 2020 Copenhagen, Denmark; URSI'19, Seville, Spain; and 23rd ICECOM 2019, Dubrovnik, Croatia. He has served or is serving as a Senior Editor of IEEE ACCESS and an Associate Editor of both IEEE TRANSACTIONS ON ANTENNAS PROPAGATION and *IEEE Antennas and Propagation Magazine*. He is the Track Chair of IEEE AP-S/URSI 2022 Denver, 2021 Singapore and 2020 Montreal; the Technical Program Committee Co-Chair of ISAP 2015, APMC 2011, and TENCON 2013; and the Publicity Chair of ICEAA/IEEE APWC 2016, IWAT 2014, and APMC 2000. His research activities are posted on the Web at http://web.science.mq.edu.au/∼esselle/ and https://www.uts.edu.au/staff/karu.esselle.

WILLIAM G. WHITTOW (Senior Member, IEEE) received the B.Sc. degree in physics and the Ph.D. degree in computational electromagnetics from the University of Sheffield, Sheffield, U.K., in 2000 and 2004, respectively.

From 2004 to 2012, he was a Research Associate with Loughborough University, Loughborough, U.K. In 2012, he became a Lecturer with the Electronic Materials Integration, University of Loughborough. He became a Senior Lecturer in 2014, a Reader (Associate Professor) in 2018, and a Professor in Radiofrequency Materials with the Wolfson School of Mechanical, Electrical and Manufacturing Engineering, Loughborough University. He is a named Investigator on EPSRC grants totaling in excess of £14m. He has authored approximately 280 peer-reviewed journal and conference papers in topics related to electromagnetic materials, synthetic dielectrics, dielectric measurements, 3-D-printing, wearable antennas, VHF antennas, specific absorption rate, finite difference time domain, specific absorption rate, metamaterials, heterogeneous substrates, embroidered antennas, inkjet printing, electromagnetic compatibility, RFID tags, phantoms, and genetic algorithms.

Prof. Whittow was the Coordinating Chair of the Loughborough Antennas and Propagation Conference from 2007 to 2011. He has served as an Associate Editor for *Electronics Letters* (IET) and also *Microwaves, Antennas and Propagation*. He serves on the technical program committees for several IEEE international conferences. He has been asked to give more than 30 invited conference presentations; a four days invited workshop on bioelectromagnetics and teaches about dielectric measurements at the European School of Antennas. In 2017, he won the Women in Engineering Men as Allies Award and he is the inaugural male Associate Fellow of Women's Engineering Society. He is a Senior Fellow of the Higher Education Academy. More than 100 of his academic journal papers can be freely downloaded here: http://publications.lboro.ac.uk/publications/all/collated/elwgw.html.